

# A Multi-wavelength study of PSR B0628-28: The first over-luminous rotation-powered pulsar?

Werner Becker<sup>1</sup>, Axel Jessner<sup>2</sup>, Michael Kramer<sup>3</sup>, Vincenzo Testa<sup>4</sup>, Clemens Howaldt<sup>1</sup>

## ABSTRACT

The ROSAT source RX J0630.8–2834 was suggested by positional coincidence to be the X-ray counterpart of the pulsar PSR B0628–28. This association, however, was regarded to be unlikely based on the computed energetics of the putative X-ray counterpart. In this paper we report on multi-wavelength observations of PSR B0628–28 made with the ESO/NTT observatory in La Silla, the Lovell telescope at Jodrell Bank and XMM-Newton. Although the optical observations do not detect any counterpart of RX J0630.8–2834 down to a limiting magnitude of  $V=26.1$  mag and  $B=26.3$  mag, XMM-Newton observations finally confirm it to be the pulsar’s X-ray counterpart by detecting X-ray pulses with the radio pulsar’s spin-period. The X-ray pulse profile is not sinusoidal but characterized by a two component pulse profile, consisting of a broad peak with a second narrow pulse leading the main pulse by  $\sim 144^\circ$ . The fraction of pulsed photons is  $(39 \pm 6)\%$  with no strong energy dependence in the XMM-Newton bandpass. The pulsar’s X-ray spectrum is well described by a power law with photon index  $\alpha = 2.63^{+0.23}_{-0.15}$ . A composite Planckian plus power law spectral model yields an interesting alternative which formally describes the observed energy spectrum equally well. Inferred from best fits are a blackbody temperature of  $\sim 1.7 \times 10^6$  K and a projected blackbody radius of  $\sim 69^{+30}_{-25}$  m, yielding a thermal flux contribution of  $\sim 20\%$  within the  $0.1 - 2.4$  keV band. The pulsar’s spin-down to X-ray energy conversion efficiency as obtained from the single power law spectral model is  $\sim 16\%$ , assuming the distance inferred from the radio dispersion measure. If confirmed, PSR B0628–28 would be the first X-ray over-luminous rotation-powered pulsar identified among all  $\sim 1400$  radio pulsars known today. The emission beam geometry of PSR B0628–28 is

---

<sup>1</sup>Max-Planck Institut für Extraterrestrische Physik, 85741 Garching bei München, Germany

<sup>2</sup>Max-Planck Institut für Radioastronomie, Effelsberg, 53902 Bad Münstereifel, Germany

<sup>3</sup>University of Manchester, Jodrell Bank Observatory, Macclesfield, Cheshire SK11 9DL, UK

<sup>4</sup>INAF - Osservatorio Astronomico di Roma, Via Frascati 33 00040 Monte Porzio Catone (Italy)

estimated from radio polarization data taken at 408 MHz and 1400 MHz. A formal best fit of the 1400 MHz data yields  $\alpha \sim 11^\circ$  for the inclination of the magnetic axis to the rotation axis and  $\beta \sim -3^\circ$  for the impact angle of the line of sight. A combination of results obtained from 408 MHz and 1400 MHz data, however, makes a nearly orthogonal solution with  $\alpha \sim 70^\circ$  and  $\beta \sim -12^\circ$  the most likely one.

*Subject headings:* pulsars:general — pulsars:individual (PSR B0628-28) — stars:neutron — stars:individual (RX J0630.8-2834) — x-ray:stars

## 1. INTRODUCTION

PSR B0628-28 is a bright radio pulsar (Large, Vaughan & Wielebinski, 1969). Its characteristic spin-down age is  $\sim 2.75 \times 10^6$  years. The pulsar’s period and period derivative are  $P = 1.24$  s and  $\dot{P} = 7.1 \times 10^{-15}$ , implying a spin-down luminosity of  $\log \dot{E} = 32.16$  erg s $^{-1}$  and a magnetic field at the neutron star poles of  $\log B_\perp = 12.48$  G. The distance to the pulsar as listed in the Princeton Pulsar Catalog (Taylor, Manchester & Lyne 1993) and the ATNF online pulsar database is 2.14 kpc (Taylor & Cordes 1993; Manchester et al. 2005). Using the NE2001 Galactic free electron density model of Cordes & Lazio (2002) which builds upon and supersedes the Taylor & Cordes (1993) model by exploiting new observations and methods, the radio dispersion measure of  $DM = 34.36$  pc cm $^{-3}$  implies that the pulsar might be closer at a distance of only 1.45 kpc. The pulsar parameters and the emission properties observed in other X-ray detected rotation-powered pulsars (cf. Becker & Trümper 1997; Becker & Aschenbach 2002 and references therein), seem to indicate that PSR B0628-28 is an ordinary, old<sup>5</sup> radio pulsar which is detectable just at the threshold of sensitivity of the current generation of X-ray observatories. The results from ROSAT and Chandra observations, however, suggest that there might be more to expect from this pulsar.

PSR B0628-28 was first noticed to have a faint potential X-ray counterpart in the ROSAT all-sky survey, RX J0630.8-2834 (Becker et al. 1993). The pulsar was therefore re-observed in October 1992 and April 1993 in two short pointed ROSAT observations of  $\sim 2.5$  ksec and  $\sim 6.3$  ksec exposures. Both observations confirmed the detection of the X-ray source RX J0630.8-2834 and collected 27 source counts from it in the ROSAT PSPC (Position Sensitive Proportional Counter). The low number of counts did not allow to

---

<sup>5</sup>in standards of X-ray detected non-recycled pulsars

obtain more than a rough hardness ratio<sup>6</sup> which suggested that RX J0630.8–2834 has a medium soft X-ray spectrum. A timing analysis was not possible either, thus leaving the association between RX J0630.8–2834 and PSR B0628–28 an open issue and based on a rough positional agreement only.

Such an association, however, was regarded to be unlikely based on the estimated energy budget of the putative X-ray counterpart. The X-ray luminosity of RX J0630.8–2834 extrapolated to the pulsar’s distance was found to be  $\sim 37\%$  of the pulsar spin-down energy. Its X-ray conversion factor thus would be few hundred times higher than the average X-ray conversion factor  $\sim 10^{-3} \dot{E}$  which is observed in the 0.1 – 2.4 keV band from other X-ray detected rotation-powered pulsars (Becker & Trümper 1997).

Follow-up optical imaging and spectroscopic observations with the ESO New Technology Telescope (NTT) in La Silla (Chile) were performed to assess the nature of the unidentified X-ray source RX J0630.8–2834. Various optical sources were identified in the  $\sim 25''$  wide ROSAT PSPC error box, which could not be conclusively ruled out as potential optical counterparts of RX J0630.8–2834.

Recently, Ögelman and Tepedelenlioglu (2002) have observed RX J0630.8–2834 as part of the Chandra-AO3 guest observer program. The source, CXC J063049.4–283443, was clearly detected with the ACIS–S<sup>7</sup> detector in an 17 ksec exposure in which 189 source counts were recorded from it. Although representing an improvement over the ROSAT observations, the low number of source counts did not support a detailed spectral analysis which could discriminate between various possible spectral models. Fixing the column absorption to a value corresponding to a neutral hydrogen density of  $1.07 \times 10^{21} \text{ cm}^{-2}$  (as deduced from the pulsar’s radio dispersion measure by assuming 10 H-Atoms per free electron), both a power law model with photon-index  $\alpha = 2.45 \pm 0.15$  and a thermal blackbody model with  $T = (4.53 \pm 0.13) \times 10^6 \text{ K}$  and  $R_{bb} \sim 1 \text{ km}$  describe the energy spectrum of CXC J063049.4–283443 equally well. As the frame time of the ACIS-S in the selected mode was close to the pulsars rotation period, a timing analysis did not yield a significant result and prevented the derivation of reliable upper limits for the fraction of pulsed photons. However, the high spatial resolution of Chandra along with its superior pointing accuracy allowed the determination of a much more accurate position of the putative X-ray counterpart RX J0630.8–2834 than before. The Chandra position of RX J0630.8–2834 was found to match the position of PSR B0628–28 by 1.5 arcsec! Any offset from the pulsar radio

---

<sup>6</sup>Ratio of the number of counts detected in the soft spectral bands vs. that detected in the hard bands.

<sup>7</sup>See [http://cxc.harvard.edu/cdo/user\\_guide.html](http://cxc.harvard.edu/cdo/user_guide.html) for a detailed description of Chandra, its instrumentation and various observing modes.

position due to its proper motion (Briskin et al. 2003) is well within the uncertainties of the Chandra position. Hence, the positional coincidence between RX J0630.8–2834 (CXC J063049.4–283443 resp.) strongly suggests that this X-ray source is indeed the counterpart of PSR B0628–28.

In this paper we report on X-ray, optical and radio observations of PSR B0628–28 which were made with XMM-Newton, the ESO NTT in La Silla and the Lovell telescope at the Jodrell Bank Observatory in order to explore the spectral and timing emission properties of this interesting pulsar. The paper is organized in the following manner: in §2 we describe the optical, radio and XMM-Newton observations of PSR B0628–28 and provide the details of the data processing and data filtering. The results of the spectral and timing analysis are given in §3. A summary and concluding discussion is presented in §4.

## 2. OBSERVATIONS AND DATA REDUCTION

### 2.1. OPTICAL OBSERVATIONS OF PSR B0628–28

Two images of 600s exposure time in the B and V filters, pointed on the position of PSR B0628–28, were made on Dec. 15, 1999 with the ESO NTT Multi-Mode Instrument (EMMI). The *B* (422.3 nm) image was taken with the blue arm, equipped with a Tektronix  $1024 \times 1024$  chip having  $24 \mu$  pixels size (0.37 arcsec), while the *V* (542.6 nm) image was acquired with the red arm mounting a Tektronix  $2086 \times 2048$  chip with  $24 \mu$  pixel size (0.27 arcsec). Two images of the Landolt field Ru149 were observed soon after for the purpose of calibrating the two images.

Bias and flat-field were applied as usual, using calibration sets acquired at evening twilight, and the reduction of the images was performed with both DAOPHOT (Stetson 1987) and SExtractor (Bertin and Arnouts, 1996) to take into account the presence of extended sources and to check the output photometry results. Photometric calibration was performed by using the Ru149 field and the average La Silla extinction terms (-0.22 for B and -0.12 for V, as found in the instrument web-page at ESO La Silla site). The night was photometric and with a good seeing, 0.75 arcsec in V.

No source is detected at the position of PSR B0628–28. Figure 1 shows a close-up view of the pulsar field as seen in the visible (V) and blue (B) bands.  $3\sigma$  upper limits assuming a point-source and correcting for the interstellar extinction are  $V = 26.1$  mag and  $B = 26.2$  mag, respectively. Values for  $E(B-V)$  were derived from dust maps (Schlegel et

al. 1998). Converting these upper limits<sup>8</sup> to a photon flux upper limit yields  $1.322 \times 10^{-7} Jy$  for the V-band and  $1.423 \times 10^{-7} Jy$  for the B-band, respectively.

## 2.2. RADIO OBSERVATIONS OF PSR B0628–28

The ephemerides for the analysis of the X-ray data were obtained from radio observations and the measurement of pulse times-of-arrival (TOAs) using the 76-m Lovell radio telescope at Jodrell Bank Observatory. Table 1 summarizes the radio ephemerides of PSR B0628–28. A dual-channel cryogenic receiver system sensitive to two orthogonal polarizations was used predominantly at frequencies close to 1400 MHz. The signals of each polarization were mixed to an intermediate frequency, fed through a multi-channel filter-bank and digitized. The data were de-dispersed in hardware and folded on-line according to the pulsar’s dispersion measure and topocentric period. The folded pulse profiles were stored for subsequent analysis. In a later off-line processing step, every sub-integration spoiled by RFI was removed, the polarizations combined and the remaining sub-integrations averaged to produce a single total-intensity profile for the observation. TOAs were subsequently determined by convolving, in the time domain, the averaged profile with a template corresponding to the observing frequency. The uncertainty on the TOA was found using the method described by Downs & Reichley (1983), which incorporates the off-pulse rms noise and the ‘sharpness’ of the template. These TOAs were corrected to the solar system barycenter using the Jet Propulsion Laboratory DE200 solar system ephemeris (Standish 1982). More details can be found in Hobbs et al. (2004). Spectral data from PSR B0628–28 were obtained from the compilation of Maron et al. (2000).

The emission beam geometry of PSR B0628–28 is not known but can be estimated from fitting the canonical rotating vector model to the polarization position angle from radio data (e.g. Lorimer & Kramer 2005). We used the polarization profiles observed at 408 MHz and 1400 MHz by Gould & Lyne (1998, see reference for details about observing set-up and calibration procedure) to determine the inclination of the magnetic axis to the rotation axis to be  $\alpha = 70^\circ$ . The impact angle of the line of sight with the magnetic axis is fitted to be  $\beta = -12^\circ$ . As usual, the small duty cycle of polarized emission available for modeling produces a distinct correlation between the fit results for  $\alpha$  and  $\beta$ . We demonstrate this by showing the  $\chi^2$ -sphere for the 1400-MHz least-squares fit in  $\alpha$  and  $\beta$  in Figure 2. Acceptable fits lie in the inside of the sickle shaped goodness of fit contours. At the higher frequency

---

<sup>8</sup>Information on the conversion from the magnitude scale to the photon flux in Jy can be found at <http://www.astro.utoronto.ca/~patton/astro/mags.htm>

of 1400 MHz shown here, the formal global minimum of the least-squares fit resides at the edge of the contours main body, in a small isolated point located at  $\alpha = 11^\circ$  and  $\beta = -3^\circ$  (cf. Figure 2). In order to decide, which solution in this rather large solution space is physically more acceptable, we can make use of the pulse shape information: the measured 50% width of the radio pulse amounts to  $\sim 17^\circ$ . From studies of a large sample of radio pulsars, one finds a relationship between the beam radius and the spin period (see Lorimer & Kramer 2005 and references therein). Based on such results, for a spin period of 1.244 s, one expects a beam width of  $\sim 11^\circ$  for a line of sight cutting through the center of the emission cone (i.e.  $\beta \sim 0^\circ$ ). An observed pulse width larger than this value may be a good indication of the possibility that the magnetic inclination angle is small, producing a path of the line-of-sight through the beam that is curved rather than straight. The fairly shallow gradient of the position angle curve may also add weight to this small- $\alpha$  solution, but a combination of the  $\chi^2$ -contours obtained for 408 MHz and 1400 MHz makes a nearly orthogonal solution  $\alpha \sim 70^\circ, \beta \sim -12^\circ$  the most likely one. A sketch which illustrates possible beam geometries is given in Figure 3.

### 2.3. XMM-NEWTON OBSERVATIONS OF PSR B0628–28

PSR B0628–28 was observed with XMM-Newton<sup>9</sup> on April 20, 2004 (XMM rev. 773) for a total on-source time of  $\sim 48\,500$  s. We used the EPIC-PN camera as the prime instrument and operated both MOS1/2 cameras in PrimeFullWindow mode to obtain imaging and spectral data. The EPIC-PN camera was setup to operate in PrimeLargeWindow readout mode which provides imaging, spectral and timing information with a temporal resolution of 48 ms. The higher temporal resolution of the EPIC-PN small-window mode would have been attractive but an overkill in view of its  $\sim 30\%$  higher dead-time (see e.g. Becker & Aschenbach 2002 for a summary of XMM-Newton instrument modes suitable for pulsar studies). The medium filter was used for the MOS1/2 cameras and the thin filter for the EPIC-PN. The expected lower efficiency of the RGS means that it is of limited use for the given exposure time. The optical field is well known from our NTT/EMMI observations so that we do not report on the analysis of XMM’s optical monitor (OM) data. This data, which were taken with the OM in standard configuration are superseded in sensitivity by our ground based ESO/NTT observation (see §2.1). A summary of exposure times, instrument modes and filters used for the X-ray observation is given in Table 2.

---

<sup>9</sup>See <http://xmm.vilspa.esa.es/> for a description of XMM-Newton, its instrumentation and the various detector modes available for observations.

XMM-Newton data have been seen to show timing discontinuities in the photon arrival times with positive and negative jumps of the order of one to several seconds (Becker & Aschenbach 2002; Kirsch et al. 2003). Inspecting the log-files from our processing of raw data we found that the EPIC-PN data of PSR B0628–28 exhibit a clock discontinuity showing one negative jump of 15s. We therefore used a release track version of the XMM-Newton SAS (Standard Analysis Software) for the analysis of the EPIC-PN data. This software detects and corrects most of the timing discontinuities during data processing. In addition, known timing offsets due to ground station and space craft clock propagation delays are corrected by this software in using new reconstructed time correlation (TCX) data. Barycenter correction of the EPIC-PN data and all other analysis steps were performed by using SAS Version 6.1.

Data screening for times of high background was done by inspecting the light-curves of the MOS1/2 and PN data at energies above 10 keV. Apart from having a rather high sky background contribution, strong X-ray emission from soft proton flares are seen at various times during the observation. Creating the light-curves with bins of 100s, we rejected those bins where the MOS1/2 light-curves had more than 130 cts/bin. For the EPIC-PN data we rejected times with more than 90 cts/bin (for comparison, data with a typical low sky background require the rejection of events at a level of  $\sim 10$  cts/bin). The data screening reduced the effective exposure time for the MOS1/2 to 35.6 ksec and 34.6 ksec, respectively. For the EPIC-PN data the effective exposure time was reduced to 31.7 ksec. The net exposure time after rejecting times of high sky background thus is only about 74% of the requested observing time.

For the spectral analysis based on the MOS1/2 data we used only those events with a detection *pattern* between 0–12 (i.e. single, double and triple events) and the *flag* parameter set to less than or equal to 1. The latter criterion excludes events which are located near to a hot pixel, or to a bright CCD column, or which are near to the edge of the CCD. For the EPIC-PN timing and spectral analyzes, we used only single and double events, i.e. those which have a pattern parameter of less than, or equal to, 4 and a flag parameter equal to zero. The energy range of the MOS1/2 and EPIC-PN CCDs was restricted to 0.2 – 10 keV for the spectral and timing analysis.

### 3. ANALYSIS OF THE XMM-DATA OF PSR B0628–28

The putative X-ray counterpart of PSR B0628–28 is detected with high significance in both the MOS1/2 and EPIC-PN data. The XMM-Newton net counting rates within the 0.2 – 10 keV band are  $0.0047 \pm 0.0008$  cts/s (MOS1),  $0.0042 \pm 0.0008$  cts/s (MOS2), and  $0.021 \pm 0.003$  cts/s (EPIC-PN), respectively. A maximum-likelihood source-detection did

not yield any evidence for a spatial extent of RX J0630.8–2834 of larger than 15 arcsec, corresponding to the HEW (Half Energy Width) of the instruments’ point spread function.

### 3.1. Timing Analysis

We used the EPIC-PN large-window mode data for the timing analysis. Given the pulsar period of  $\sim 1.244$ s the temporal resolution of 48ms allows us to perform a detailed timing analysis in searching for X-ray pulsations and to construct a pulse profile with up to  $\sim 26$  independent phase bins, if supported by the photon number statistics.

Events were selected from a circle of 25 arcsec radius centered on RX J0630.8–2834. This extraction region contains 80% of the point source flux. For the barycenter correction we applied the standard procedures for XMM-Newton data using *barycen-1.17.3* and the JPL DE200 Earth ephemeris (Standish 1982) to convert photon arrival times from the spacecraft to the solar system barycenter (SSB) and the barycentric dynamical time (TDB). The pulsar radio timing position (cf. Table 1) was used for the barycenter correction. The spin-parameters  $f$  and  $\dot{f}$  of PSR B0628–28 are known with high precision from our contemporaneous radio observations, covering the mean epoch MJD=53063.4104692111723 (TDB@SSB) of the XMM-Newton observation. PSR B0628–28 is not known to show timing irregularities (glitches) so that we can fold the photon arrival times using the pulsar’s radio ephemeris (see Table 1). The statistical significance for the presence of a periodic signal was obtained from a  $Z_n^2$ -test with 1 – 10 harmonics in combination with the H-Test to determine the optimal number of harmonics (De Jager 1987; Buccheri & De Jager 1989). The optimal number of phase bins for the representation of the pulse profile was determined by taking into account the signal’s Fourier power and the optimal number of harmonics deduced from the H-Test (see Becker & Trümper 1999 and references therein).

Within the 0.2 – 10 keV energy band, 1290 events were available for the timing analysis of which  $\sim 35\%$  are estimated to be background. The  $Z_n^2$ -test gave 66.1 for  $n = 4$  harmonics ( $Z_1^2 = 48.41$ ). According to the H-Test, the probability of measuring  $Z_4^2 = 66.1$  by chance is  $\sim 3 \times 10^{-11}$  thus confirming RX J0630.8–2834 (CXC J063049.4–283443, resp.) to be the counterpart of PSR B0628–28 and establishing it firmly to be an X-ray pulsar!

Figure 4 depicts the X-ray pulse profile of PSR B0628–28 for the 0.2 – 10 keV energy band. As indicated by the higher harmonic content and as can be seen easily in the figure, the pulse shape is not sinusoidal but double peaked, with a main broad peak of width  $\sim 180^\circ$  and a narrow pulse component of  $\sim 45^\circ$  width longitude. By taking the center of mass of both pulse components as a reference point, the separation in phase between both peaks is



$\sim 0.4$  ( $144^\circ$  longitude). The fraction of pulsed events in the  $0.2 - 10$  keV energy range is determined to be of  $39 \pm 6\%$  by using a bootstrap method (Swanepoel, de Beer & Loots 1996; Becker & Trümper 1999). Restricting the timing analysis to the  $0.2 - 1.0$  keV and  $1.0 - 2.1$  keV energy bands yields the pulsed fractions  $41 \pm 7\%$  and  $42 \pm 10\%$ , respectively, which do not indicate a significant energy dependence over the  $0.2 - 10$  keV bandpass, although the decreasing signal to noise ratio beyond  $\sim 2.1$  keV makes any conclusion for this energy band merely tentative.

Comparing the X-ray pulse profile with the one taken with the Jodrell Bank radio telescope at 1.4 GHz shows that both profiles are markedly different. Measuring the TOAs of the radio and X-ray pulses shows that the narrow X-ray pulse leads the radio pulse by  $\sim 0.2$  ( $72^\circ$  longitude) in phase. The radio pulse itself leads the broader X-ray pulse by about the same amount of  $72^\circ$  longitude. The arrival of the radio pulse thus appears to be in the middle between the arrival of the two X-ray pulse components.

We note that uncertainties of the XMM-Newton clock against UTCs are not relevant as those are on a scale of  $\sim 100 \mu s$  (Becker et al. 2005, in prep.) and thus are a factor of  $\sim 1000$  smaller than the bin width of the X-ray pulse profile shown in Figure 4.

### 3.2. Spectral Analysis

The energy spectrum of PSR B0628–28 was extracted from the MOS1/2 data by selecting all events detected in a circle of radius 50 arcsec centered on the pulsar position. Using the XMM-Newton/EPIC-MOS model point spread function, 90% of all events of a point source are within this region. The background spectrum was extracted from an annulus of outer radius 85 arcsec surrounding PSR B0628–28. For the EPIC-PN data we used an extraction radius of 31 arcsec centered on PSR B0628–28. This selection region includes  $\sim 85\%$  of the point source flux. As the instrument focus is relatively close to the edge of the PN-CCD, we extracted the background spectrum from a source free region about one arc-minute east of the pulsar. Out-of-time events prevent us from extracting the background spectrum from a region located below the source and along the CCD read-out direction.

In total, the extracted spectra include 814 source counts from the EPIC-PN camera and 430 source counts from the EPIC-MOS1/2 detector. The spectral data were dynamically binned so as to have at least 30 counts per bin. Model spectra were then simultaneously fit to both the PN and MOS1/2 data.

Amongst the single component spectral models, a power law model was found to give the statistically best representation ( $\chi^2=34.6$  for 37 dof) of the observed energy spectrum.

A single blackbody model did not give acceptable fits ( $\chi^2=65.1$  for 37 dof) and can be rejected. The power law model yields a column absorption of  $N_H = 6.0_{-1.8}^{+3.1} \times 10^{20} \text{ cm}^{-2}$ , a photon-index  $\alpha = 2.63_{-0.15}^{+0.23}$  and a normalization of  $1.0_{-0.1}^{+0.13} \times 10^{-5} \text{ photons cm}^{-2} \text{ s}^{-1} \text{ keV}^{-1}$  at  $E = 1 \text{ keV}$ . The errors represent the  $1\sigma$  confidence range for one single parameter of interest. For the unabsorbed energy flux we measured  $f_x = 3.36_{-0.17}^{+0.22} \times 10^{-14} \text{ ergs s}^{-1} \text{ cm}^{-2}$  in the  $0.5 - 10 \text{ keV}$  band, yielding an X-ray luminosity of  $L_x = 8.42_{-0.54}^{+0.42} \times 10^{30} \text{ ergs s}^{-1}$  for a distance of 1.45 kpc. For the ROSAT energy band,  $0.1 - 2.4 \text{ keV}$ , we measured the flux to be  $f_x = 9.4_{-2.3}^{+5.0} \times 10^{-14} \text{ ergs s}^{-1} \text{ cm}^{-2}$ , yielding an X-ray luminosity of  $L_x = 2.4_{-0.6}^{+1.25} \times 10^{31} \text{ ergs s}^{-1}$ . These luminosities imply the huge rotational energy to X-ray energy conversion factors  $L_x/\dot{E} = 58.3 \times 10^{-3}$  within  $0.5 - 10 \text{ keV}$  and  $163.4 \times 10^{-3}$  if transformed to the ROSAT band (see §4 for a discussion).

The best-fit power law spectrum and residuals are shown in Figure 5. Contour plots showing the relationship between the photon index and the column absorption for various confidence levels are shown in Figure 6.

Testing composite spectral models consisting of two Planckian components or of a Planckian plus power law component resulted in fits which had a chi-square of 28.6 (for 35 dof), i.e. a goodness comparable to what we found in the single component power law fit. The F-test statistic for adding the extra blackbody spectral component to the power law model yields a probability of only 97.2%, i.e. slightly more than  $2\sigma$ . The justification to include a thermal component to the power law spectrum thus is not particularly strong by statistical means.

The parameters fitted for the composite Planckian plus power law model are a column absorption of  $N_H \leq 2.5 \times 10^{20} \text{ cm}^{-2}$ , a photon-index  $\alpha = 2.27_{-0.13}^{+0.23}$  and a normalization of the power law component of  $4.8_{-0.9}^{+1.6} \times 10^{-6} \text{ photons cm}^{-2} \text{ s}^{-1} \text{ keV}^{-1}$  at  $E = 1 \text{ keV}$ . The blackbody temperature and the size of the projected emitting area are  $kT = 0.25_{-0.04}^{+0.05} \text{ keV}$  and  $R_{bb} = 69_{-25}^{+30} \text{ m}$ , assuming a pulsar distance of 1.45 kpc. For the unabsorbed energy flux and luminosity we compute  $f_x = 2.8_{-1}^{+3} \times 10^{-14} \text{ erg s}^{-1} \text{ cm}^{-2}$  and  $L_x = 7.0_{-2}^{+8} \times 10^{30} \text{ erg s}^{-1}$  for the  $0.5 - 10 \text{ keV}$  band. For the  $0.1 - 2.4 \text{ keV}$  energy band we compute the model flux to be  $f_x = 4.0_{-1.7}^{+6.0} \times 10^{-14} \text{ erg s}^{-1} \text{ cm}^{-2}$ , yielding an X-ray luminosity of  $L_x = 1.0_{-0.5}^{+1.5} \times 10^{31} \text{ erg s}^{-1}$ . The rotational energy to X-ray energy conversion factors obtained from this combined model are  $L_x/\dot{E} = 48.4 \times 10^{-3}$  within  $0.5 - 10 \text{ keV}$  and  $69.8 \times 10^{-3}$  if transformed to the ROSAT band.

In computing the relative contributions of the thermal and non-thermal spectral components we find that for the best fitting parameters  $\sim 20\%$  of the X-ray flux within the  $0.1 - 2.4 \text{ keV}$  band could be of thermal origin and emitted from heated polar caps. In stretching the errors to the limits, however, a maximum of up to  $\sim 100\%$  thermal flux can

not be excluded for this energy band. At higher and lower energies non-thermal emission will dominate though. Figure 7 illustrates the relative contributions of the thermal and non-thermal spectral components as indicated by the best fitting model parameters.

Defining the size of a presumed polar cap as the foot points of the neutron star’s dipolar magnetic field, the radius of the polar cap area is given by  $\rho = \sqrt{2\pi R^3/cP}$  with  $R$  being the neutron star radius,  $c$  the velocity of light and  $P$  the pulsar rotation period (see e.g. Michel 1991). For PSR B0628–28 with a rotation period of 1.244 s this yields a polar cap radius of  $\rho \sim 130$  m which is not too different from the size of the blackbody emitting area fitted in the composite blackbody plus power law model for an assumed distance of 1.45 kpc.

The two component blackbody model would yield an alternative description of the spectrum as well, based on thermal emission mechanisms only. The parameters fitted by this model are a column absorption of  $N_H \leq 0.9 \times 10^{20} \text{ cm}^{-2}$ , blackbody temperatures of  $kT_1 = 0.142_{-0.01}^{+0.22}$  keV,  $kT_2 = 0.402_{-0.04}^{+0.09}$  keV, and radii of the projected emitting areas of  $R_1 = 278.8_{-59.2}^{+116.4}$  m,  $R_2 = 34.8_{-11.33}^{+9.75}$  m.

With a spin-down age of  $\sim 2.7 \times 10^6$  years PSR B0628–28 should still have some residual heat content from its birth event. Depending on the equation of state the surface temperature could be in the range  $\sim 1 - 3 \times 10^5$  K (cf. Becker & Pavlov 2002 and references therein) and then would contribute on a low level to the detected soft X-ray emission. Clearly, the power law spectral model fit does not require this extra thermal component by statistical means but to estimate the upper limit for the surface temperature of PSR B0628–28 we have added a blackbody component to the best fitting power law model. We then calculated the confidence ranges of the blackbody normalization and temperature by leaving all other parameters free. The resulting contours, computed for two parameters of interest, are shown in Figure 8. For the thermal emission to be emitted from the whole surface of a neutron star of radius 10 km we find a  $2\sigma$  surface temperature upper limit of  $T_s^\infty < 5.3 \times 10^5$  K which is somewhat above the temperatures predicted by cooling models (e.g. Page & Applegate 1992; Yakovlev et al. 1999).

The spectral parameters of the various models fitted to the energy spectrum of PSR B0628–28 are summarized in Table 3.

### 3.3. Multi-wavelength Spectrum

In order to construct a broadband spectrum combining all spectral information available from PSR B0628–28 we adopted the radio spectrum from Maron et al. (2000) and plotted it in Figure 9 together with the optical V- and B-band upper limits from our ESO/NTT

observations and the XMM-Newton observed pulsar spectrum. The radio spectrum has been measured up to 10.6 GHz and can be modeled by a simple power-law with an average photon index of  $-2.9 \pm 0.1$  (Maron et al. 2000), even though in contrast to measurements reported by Reyes et al. (1995), the spectrum does show a turn-over at low frequencies (see Maron et al. 2000 and references therein). The flux density in the radio part of the spectrum, which is supposed to be due to coherent radiation, is several orders of magnitude greater than the extrapolated optical or X-ray flux densities.

Extrapolating the power law spectrum which describes the XMM-Newton data to the optical V- and B-bands yields a photon flux which exceeds the measured upper limits by more than an order of magnitude. This suggests that the broadband spectrum, if entirely non-thermal, has to break somewhere before or in the soft channels of the X-ray spectrum. To test this hypothesis we have fitted a broken power law model to the XMM-Newton data and found it providing a better description ( $\chi^2 = 27.576$  for 37 dof) of the observed X-ray spectrum than the single power law model does. A broken power law model which is in agreement with the optical V- and B-band upper limits and the XMM-Newton data has its break point fitted at  $E_{break} = 0.85^{+0.13}_{-0.16}$  keV. The photon-index for  $E < E_{break}$  and  $E > E_{break}$  is found to be  $\alpha_1 = 1.45^{+0.04}_{-0.003}$  and  $\alpha_2 = 2.71^{+0.34}_{-0.26}$ , respectively, with a normalization of  $1.6 \times 10^{-5}$  photons  $\text{cm}^{-2} \text{s}^{-1} \text{keV}^{-1}$  at 1 keV. The column absorption is compatible with an upper limit of  $N_H = 1.5 \times 10^{20} \text{cm}^{-2}$ . The errors represent the  $1 - \sigma$  confidence range calculated for two parameters of interest.

#### 4. DISCUSSION & SUMMARY

We have investigated the optical and X-ray emission properties of RX J0630.8–2834 and identified it to be the X-ray counterpart of the old rotation-driven pulsar PSR B0628–28 by detecting its X-ray pulses at the radio pulsar’s spin frequency. Its X-ray pulse profile is characterized by a single broad peak and a second narrow pulse component which leads the main pulse by  $\sim 144^\circ$ . A comparison of the pulse profiles observed in the 0.2 – 10 keV band and at 1.4 GHz shows that the X-ray pulse profile is markedly different from the single narrow peaked profile observed in the radio band. The XMM-Newton observed pulsed fraction is  $(39 \pm 6)\%$  with no strong energy dependence in the 0.2 – 10 keV bandpass. The pulsar’s X-ray spectrum is very well described by a power law spectrum, indicating that non-thermal radiation processes dominate the pulsar’s X-ray emission in the 0.2 – 10 keV band. A  $\sim 20\%$  thermal flux contribution from heated polar caps is inferred from the best fitting parameters of a combined power law plus Planckian spectrum.

The emission beam geometry of PSR B0628–28 is estimated from radio polarization

data taken at 408 MHz and 1400 MHz. A formal best fit of the 1400 MHz data yields  $\alpha \sim 11^\circ$  for the inclination of the magnetic axis to the rotation axis and  $\beta \sim -3^\circ$  for the impact angle of the line of sight. A combination of results obtained from 408 MHz and 1400 MHz data, however, makes a nearly orthogonal solution with  $\alpha \sim 70^\circ$  and  $\beta \sim -12^\circ$  the most likely one. We would like to point out, however, that in the case the beam geometry would be  $\alpha \sim 11^\circ$ ,  $\beta \sim -3^\circ$  (which currently can not be ruled out) it would disclose us a full view of the pulsar polar cap.

Comparing the pulsar’s X-ray luminosity,  $L_x(0.1-2.4 \text{ keV}) = 2.36_{-0.57}^{+1.25} \times 10^{31} \text{ ergs s}^{-1}$ , as inferred by the power law spectral model and estimated under the assumption of a pulsar distance of 1.45 kpc, with the pulsar’s spin-down energy,  $\dot{E} = 1.445 \times 10^{32} \text{ erg/s}$ , we find that PSR B0628–28 emits the huge amount of  $\sim 16\%$  of its spin-down energy into the soft X-ray band. If confirmed, PSR B0628–28 would be the first X-ray over-luminous rotation powered pulsar identified among all  $\sim 1400$  radio pulsars known today. It is not known what could cause such a high X-ray luminosity. Among the most possible scenarios are extreme re-heating from vortex creep, accretion from the ISM, decay of the pulsar magnetic field, or extreme polar cap heating (cf. Harding & Muslimov 2001,2002), though all this is not observed so far in any of the other X-ray detected rotation powered pulsars.

Well known pulsars which, according to their timing parameters, fall into the same category as PSR B0628–28 are PSRs B1929+10, B0950+08, B0823+26 and J2043+2740. All four have been detected by ROSAT and ASCA at the limits of their sensitivity and have been investigated using XMM-Newton recently (Becker et al. 2004; 2005), but none of them shows evidence for the X-ray over-luminosity observed in PSR B0628–28. Thus, is PSR B0628–28 unique among all known rotation powered pulsars? At least its observed spectral and temporal emission properties do not support this view. The results found for PSRs B1929+10, B0950+08, B0823+26 and J2043+2740 are all in line with the emission properties observed in PSR B0628–28. As for PSR B0628–28, the X-ray emission from these old pulsars seems to be dominated by non-thermal radiation processes. None of the observed spectra *required* adding a thermal component consisting of either a hot polar cap or surface cooling emission to model the data. The X-ray spectrum of PSR B0950+08 is best described by a single power law of photon-index  $\alpha = 1.93_{-0.12}^{+0.14}$ . Its X-ray emission is pulsed with two peaks per period and a phase separation of  $\sim 144^\circ$  between the two pulse components. Its pulsed fraction is  $(28 \pm 6)\%$  in the 0.2 – 10 keV band. The spectral and temporal emission properties observed from PSR B1929+10 and PSR B0823+26 are very similar to those seen in PSR B0950+08 and PSR B0628–28(Becker et al. 2004). Their energy spectra can be adequately described by a single power law with photon-index  $\alpha = 2.72_{-0.09}^{+0.11}$  and  $\alpha = 2.5_{-0.45}^{+0.9}$ , respectively. Fitting combined Planckian plus power law models to the observed spectral data from these pulsars, however, is possible as well and indicates thermal

contributions from heated polar caps to the soft X-ray bands of the order of  $\sim 10 - 40\%$  according to the best fitting model spectra. The fraction of pulsed photons for all these pulsars are in the range of  $\sim 30 - 50\%$ .

The similarity in the emission properties to other X-ray detected pulsars from the same class does not support the assumption that there is anything special in the emission properties of PSR B0628–28 which justifies the high spin-down to X-ray energy conversion. The spin-down to X-ray energy conversion efficiency for the sample of ROSAT detected rotation-powered pulsars was investigated by Becker & Trümper (1997) who described the available data with the relation  $L_x \sim 10^{-3} \dot{E}$ . This relation is corrected for possible thermal contributions e.g. in cooling neutron stars and was found to fit the data within the 0.1 – 2.4 keV band assuming isotropy. Arguing that the 2 – 10 keV energy band should be better suited for this study because any thermal contribution and spectral fitting uncertainties from interstellar absorption is minimized, Possenti et al. (2002) performed a similar analysis using ROSAT, ASCA and BeppoSAX data of a somewhat larger sample than was available before. For faint sources like the old and nearby radio pulsars and most millisecond pulsars, Possenti et al. (2002) obtained the flux in the 2 – 10 keV band by simply upscaling the ROSAT results from Becker & Trümper(1997). Those results, however, are not very meaningful, especially if there is no spectral information available and a simple counts-to-energy conversion requires the assumption of a spectral shape, as it was the case for the sample of old non-recycled pulsars. Here, PSR B1929+10 was taken as a prototype and X-ray fluxes were obtained by assuming that the X-ray emission from old pulsars originates entirely from heated polar caps. Our new spectral results obtained for PSR B0628–28 and for the other old rotation-powered pulsars in recently XMM-Newton observations (cf. Becker et al. 2004; 2005), however, shows that this assumption is no longer valid.

Consequently, we do not follow their conclusions e.g. of maximum X-ray emissivity but assume that the conversion efficiency  $L_x/\dot{E}$  for PSR B0628–28 within 0.1 – 2.4 keV is in the same range of  $x = (0.5 - 5) \times 10^{-3}$  than observed by Becker et al. (2004; 2005) in PSR B1929+10 ( $3.44 \times 10^{-3}$ ), B0950+08 ( $2.85 \times 10^{-4}$ ), B0823+26 ( $5.1 \times 10^{-4}$ ), and J2043+2740 ( $5 \times 10^{-4}$ ) using XMM-Newton. We are therefore in favor of the interpretation that in  $L_x = 4\pi d_{DM}^2 f_x$  the distance of 1.45 kpc, based on the radio dispersion measure and the Galactic free electron density model NE2001 (Cordes & Lazio 2002), is overestimated.

If we take the errors in the X-ray flux measured from PSR B0628–28 into account, we obtain a pulsar distance  $d(x) = \sqrt{\dot{E}x/4\pi f_x}$  which is about 5 to 22 times closer than the radio dispersion measure inferred distance. Table 4 summarizes the scaling parameters which were computed for the measured soft X-ray flux but with assumed spin-down conversion efficiencies.

Distances based on the NE2001 Galactic free electron density model are estimated to be, on average, correct within a factor of  $\sim 20\%$ . However, as the Galactic free electron distribution is seen to vary significantly on small and large scales by more than two orders of magnitude it might not be excluded that for single pulsars the model can over- or underestimate the free electron density and thus yields a wrong distance estimate. Although it is difficult to imagine that the model predicted distance is off by a factor 10 to 20, a factor of  $\sim 3 - 5$  might not be excluded in rare cases.

For example, for a pulsar distance of 300pc the NE2001 model predicts a dispersion measure  $DM = \int_0^{300pc} n_e dl$  of  $4.25 \text{ pc cm}^{-3}$ . If compared with the measured value of  $34.36 \text{ pc cm}^{-3}$  this means that any extra unmodeled material along the line of sight to PSR B0628–28 would need to contribute a radio dispersion measure of  $\sim 30 \text{ pc cm}^{-3}$ . This correction would not necessarily be due to an unmodeled H-II region (typically  $DM \sim 1000 \text{ pc cm}^{-3}$ ) but would be only slightly higher than, but still comparable to the typical "clump" added in the NE2001 model for discrepant lines of sight, e.g. towards PSR J1031-6117, PSR J1119-6127, and PSR J1128-6219 (Cordes & Lazio 2003). Although these "clumps" in the NE2001 model do not necessarily represent physical objects, we did inspect the Digitized Sky Survey images and the images from our ESO/NTT observations to see whether they show any evidence of enhanced diffuse emission near to the region of PSR B0628–28. No noticeable source was recognized that could account for this extra correction. Inspecting the Southern H-Alpha Sky Survey Atlas (Gaustad et al. 2001) revealed some indications on a larger scale of  $\sim 10^\circ$  for a H-II region to the north of PSR B0628–28, but it is unlikely that this could affect the distance estimate by a factor of 5 to 10 or even more (J.Lazio priv. com.).

One way to evaluate a possible range of distances is by comparing the transverse velocity, derived from the measured proper motion and an assumed distance, to typical pulsar velocities. For instance, for the 1.45 kpc inferred from NE2001, the proper motion measurement of  $48.7 \text{ mas yr}^{-1}$  (Hobbs et al. 2004) translates into a transverse speed of  $335 \text{ km s}^{-1}$  which compares to a mean 2-D speed as found for a large sample of pulsars of  $246 \pm 22 \text{ km s}^{-1}$  (Hobbs et al. 2005). For the larger distance of 2.15 kpc derived using the Taylor & Cordes (1993) model, the velocity increases to a rather large but still plausible value of  $497 \text{ km s}^{-1}$ . If the pulsar were a factor of 5 or 22 closer, than the transverse speed drops to  $67 \text{ km s}^{-1}$  and  $15 \text{ km s}^{-1}$ , respectively. Unless the non-measurable radial speed happens to be large, the latter velocity is extremely small and quite unlikely.

Although the distance of the pulsar might be the most obvious parameter which may lead to a too high X-ray conversion efficiency, there might be others. The conversion efficiency here and in Becker & Trümper (1997) is for isotropy. Would it be possible that the pulsar

has an atypically small beaming angle? or that it could be a coaction of several effects like beaming, distance, peculiarities of its magnetosphere which cause the apparent higher X-ray efficiency?

So far PSR B0628–28 was not included in any radio parallax measurement program. The pulsar’s radio emission is strong enough so that a radio parallax could be measured with the VLBA. This will be done on a time scale of about two years and will provide us with the missing information on whether it is ”simply” the pulsar distance which causes the inferred huge X-ray conversion or whether PSR B0628–28 bears more interesting things to discover.

## REFERENCES

- Becker, W., Kramer, M., Jessner, A., Taam, R.E., Jai, J.J., Cheng, K.S., Mignani, R., Pellizzoni, A., de Luca, A., Slowikowska, A., Caraveo, P., 2005, ApJ submitted, (astro-ph/0506545)
- Becker, W., Weisskopf, M.C., Tennant, A.F., Jessner, A., Dyks, J., Harding, A.K., Zhang, S.N., 2004, ApJ, 615, 908
- Becker, W., Aschenbach, B., 2002, in Proceedings of the WE-Heraeus Seminar on Neutron Stars, Pulsars and Supernova remnants, Eds. W.Becker, H.Lesch & J.Trümper, MPE-Report 278, 64, (available from astro-ph/0208466)
- Becker, W., Pavlov, G.G., 2001, in *The Century of Space Science*, Eds. J.Bleeker, J.Geiss & M.Huber, Kluwer Academic Publishers, p721 (available from astro-ph/0208356).
- Becker, W. & Trümper, J. 1999, A&A, 341, 803
- Becker, W., Trümper, J., 1997, A&A, 326, 682
- Becker, W., 1994, PhD Thesis, Ludwig-Maximilian-University of Munich,
- Becker, W., Trümper, J. & Ögelman, H., 1993, *Search for cooling neutron stars in the ROSAT survey*, in *Isolated Pulsars*, eds K.A. Van Riper, R.I. Epstein & C. Ho, 104-109, Cambridge University Press
- Bertin, E., Arnouts, S., 1996, A& AS, 117, 393
- Briskin, W.F., Fruchter, A.S., Goss, W.M., Herrnstein, R.M., Thorsett, S.E., 2003, ApJ, 126, 3090
- Cordes, J.M., Lazio, T.J.W., 2002, astro-ph/0207156



- Cordes, J.M., Lazio, T.J.W., 2003, astro-ph/0301598
- Downs, G.S., Reichley, P.E., 1983, ApJS, 53,169
- Gaustad, E., McCullough, P.R., Rosing, W., Van Buren, D., 2001, PASP, 113, 1326
- Gould, D.M., Lyne, A.G., 1998, MNRAS, 301, 235
- Harding, A.K., Muslimov, A.G.,2001, ApJ, 556, 1001
- Harding, A.K., Muslimov, A.G.,2002, ApJ, 568, 862
- Hobbs, G., Lyne, A. G., Kramer, M., Martin, C. E., Jordan, C. A., 2004, MNRAS, 353, 1311
- Hobbs, G., Lorimer, D. R., Lyne, A. G., Kramer, M., 2005, MNRAS (in press, astro-ph/0504584)
- Kirsch, M.G.F., Becker, W., Benlloch-Garcia, S., et al., in *X-Ray and Gamma-Ray Instrumentation for Astronomy XIII*, eds Flanagan, K.A. & Siegmund, O.H.W., 2004, SPIE, Volume 5165, 85
- Lorimer, D.R., Kramer, M., 2005, Handbook of Pulsar Astronomy, CUP, Cambridge
- Manchester, R., Hobbs, G., Teoh, A., Hobbs, M., 2005, ApJ, 129, 1993
- Maron et al., 2000, Astron. Astrophys. Suppl. Ser., 147, 195
- Michel, F.C., 1991, *Theory of Neutron Star Magnetospheres*, University of Chicago Press, Chicago, IL
- Large, M. I., Vaughan, A.E., Wielebinski, R., 1969, Nature, 223, 1249
- Ögelman, H.B., Tepedelenlioglu, E., 2003, AdSpR, Volume 33, Issue 4, 597
- Page, D., Applegate, J.L. 1992, ApJ, 394, L17
- Reyes, F., Aparici, J., Olmos, F., 1995, A&A, 301, 182
- Schlegel, D., Finkbeiner, D., Davis, M., ApJ, 1998, 500, 525.
- Standish, E.M., 1982, A&A, 114 ,297
- Stetson, P.B., 1987, PASP, 99, 191
- Taylor, J.H., Cordes, J. M., 1993, ApJ, 411, 674

Taylor, J.H., Manchester R.N., Lyne, A.G., 1993, ApJS., 88, 529

Yakovlev, D.G., Levenfish, K.P., Shibano, Yu.A., 1999, Physics-Uspekhi, 169, 825

WB acknowledges that a significant part of the XMM-data analysis of PSR B0628-28 was done during the workshop on *High Energy Phenomena of Compact Objects* which was held from March 7 – 18 2005 at the Theoretical Institute for Advanced Research in Astrophysics (TIARA) in Hsinchu/Taiwan. WB further acknowledges discussion with R.Mignani, J.M. Cordes and T.J.W. Lazio. We are grateful to Olaf Maron for the use of his database of pulsar radio fluxes. Optical observations were made with ESO Telescopes at the La Silla Observatories under program 64.N-0698. We thank the anonymous referee for thoroughly reading the manuscript and the many useful comments.

Table 1. Ephemerides of PSR B0628–28

Right Ascension (J2000)	$06^h30^m49^s.417 \pm 00^s.006$
Declination (J2000)	$-28^d34^m42^s.91 \pm 00^s.1$
First date for valid parameters (MJD)	52956
Last date for valid parameters (MJD)	53256
Infinite-frequency geocentric pulse arrival time (MJD, UTC) <sup>a</sup>	53106.000013822
Pulsar rotation period (s)	1.24442260399
Pulsar rotation frequency ( $s^{-1}$ )	0.8035855317903
First derivative of pulsar frequency ( $s^{-2}$ )	$-4.61639 \times 10^{-15}$
Second derivative of pulsar frequency ( $s^{-3}$ )	$5.30 \times 10^{-29}$
Spin-down age (yr/ $10^6$ )	2.754
Spin-down energy (erg/s/ $10^{32}$ )	1.445
Inferred Magnetic Field ( $G/10^{12}$ )	3.02
Dispersion Measure (pc/cm <sup>3</sup> )	34.36
Distance <sup>b</sup> (kpc)	1.45

Note. —

<sup>a</sup> The integer part of this time is the barycentric (TDB) epoch of RA, DEC,  $f$ ,  $\dot{f}$ ,  $\ddot{f}$ .

<sup>b</sup> Dispersion-measure inferred distance according to Cordes and Lazio (2002).

Table 2. Instrument setups, filter usage, start time, durations, and effective exposures of the XMM-Newton observations of PSR B0628–28.

Detector	Mode	Filter	Start time (UTC)	Duration (s)	eff. Exp. (s)
EMOS1	PrimeFullWindow	Medium	2004-02-28T02:20:13	48 463	35 568
EMOS2	PrimeFullWindow	Medium	2004-02-28T02:20:10	48 471	34 590
EPN	PrimeLargeWindow	Thin	2004-02-28T02:39:43	46 998	31 738

Table 3. Models and parameters as fitted to the XMM-Newton observed X-ray spectrum of PSR B0628–28

model <sup>a</sup>	$\chi^2_\nu$	$\nu$	$N_H/10^{20}$ $\text{cm}^{-2}$	$\alpha / kT^b$	Normalization at 1 keV Photons/keV/cm <sup>2</sup> /s	Radius <sup>c</sup> m
PL	0.926	37	$6.0^{+3.0}_{-1.8}$	$2.63^{+0.22}_{-0.15}$	$1.0^{+0.13}_{-0.1} \times 10^{-5}$	
BB	1.749	37	$\leq 0.2$	$0.23^{+0.01}_{-0.01}$		$131.7^{+13.8}_{-12.5}$
BB+BB	0.808	35	$\leq 0.9$	$kT_1 = 0.142^{+0.22}_{-0.01}$ $kT_2 = 0.402^{+0.09}_{-0.04}$		$278.8^{+116.4}_{-59.2}$ $34.8^{+9.75}_{-11.33}$
BB+PL	0.810	35	$\leq 2.5$	$2.27^{+0.23}_{-0.13} / 0.25^{+0.05}_{-0.04}$	$4.8^{+1.6}_{-0.9} \times 10^{-6}$	$69^{+30}_{-25}$
BB+PL	0.969	35	$6.4^{+4.6}_{-1.4}$	$2.26^{+0.3}_{-0.2} / < 0.053$	$1.0^{+0.2}_{-0.1} \times 10^{-5}$	10 000
BKNPL	0.935	37	$\leq 1.4$	$\alpha_1 = 1.478^{+0.02}_{-0.02}$ $\alpha_2 = 2.7215^{+0.4}_{-0.3}$	$1.2^{+0.2}_{-0.1} \times 10^{-5}$	

Note. — <sup>a</sup> BB = blackbody; PL = power law; BKNPL = broken power law. Errors represent the  $1\sigma$  confidence range. For single component spectral models errors were computed for one parameter of interest. For composite models the errors were computed for two parameters of interest.

<sup>b</sup> The entry in this column depends on the spectral model — it is the power law photon index  $\alpha$  or the temperature  $kT$  in keV

<sup>c</sup> For thermal models for which we computed or fixed the radius of the emitting area we assumed a pulsar distance of 1.45 kpc.

Table 4. Distance scales of PSR B0628–28 for assumed spin-down luminosity to X-ray conversion factors  $L_x/\dot{E}$

$L_x/\dot{E}$	$f_x(0.1 - 2.4 \text{ keV})$ erg/s/cm <sup>2</sup>	$d$ pc	$d_{DM}/d$
$5 \times 10^{-3}$	$7.1394 \times 10^{-14}$	290.8	4.98
$5 \times 10^{-3}$	$9.4194 \times 10^{-14}$	253.3	5.72
$5 \times 10^{-3}$	$14.412 \times 10^{-14}$	204.7	7.07
$10^{-3}$	$7.1394 \times 10^{-14}$	130.1	11.13
$10^{-3}$	$9.4194 \times 10^{-14}$	113.3	12.78
$10^{-3}$	$14.412 \times 10^{-14}$	91.5	15.82
$5 \times 10^{-4}$	$7.1394 \times 10^{-14}$	92.9	15.58
$5 \times 10^{-4}$	$9.4194 \times 10^{-14}$	80.1	18.08
$5 \times 10^{-4}$	$14.412 \times 10^{-14}$	64.7	22.38

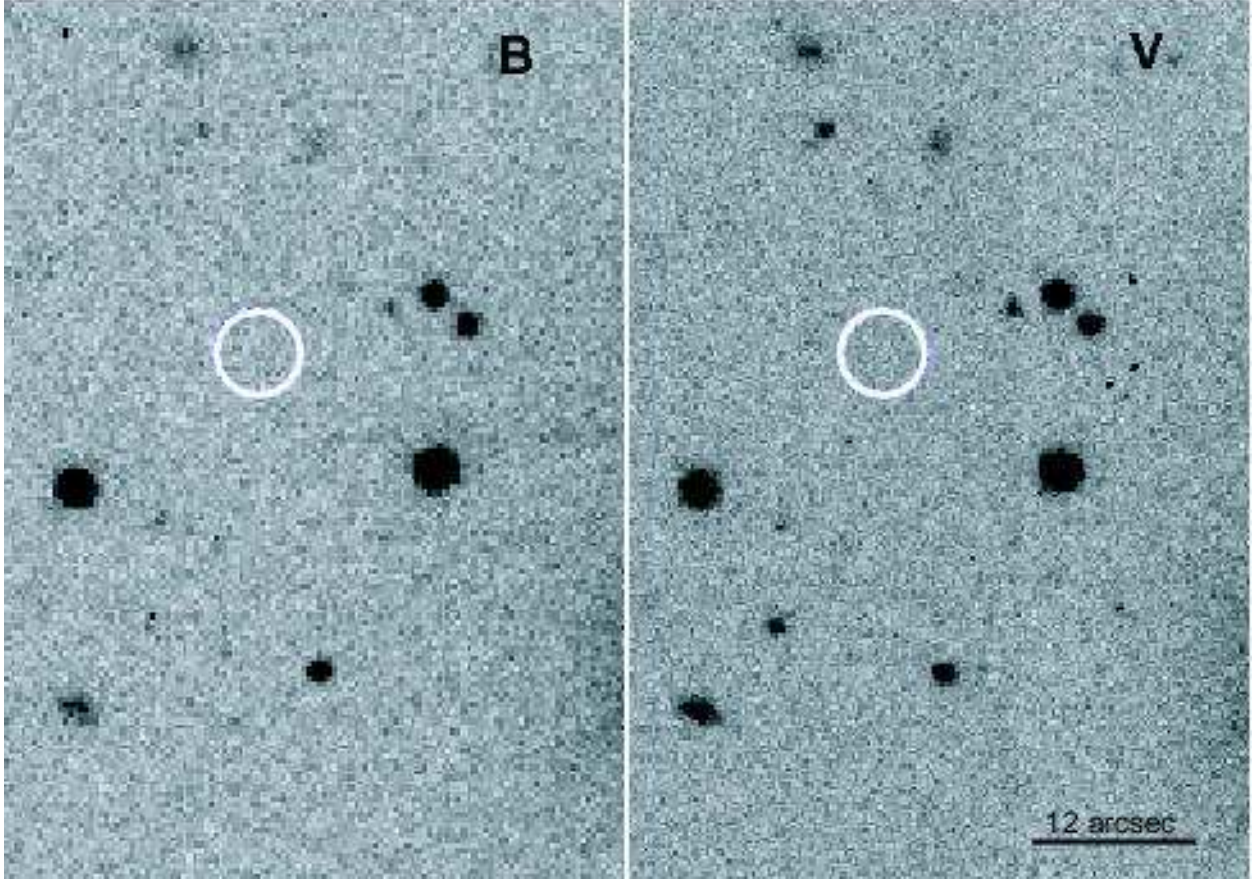


Fig. 1.— The visible sky around PSR B0628–28 as seen with the ESO NTT/EMMI telescope/detector in La Silla using the V (542.6 nm) and B (422.3 nm) band filters. The circles have a radius of 3 arcsec and are centered at the pulsar position. Top is north and left is east.

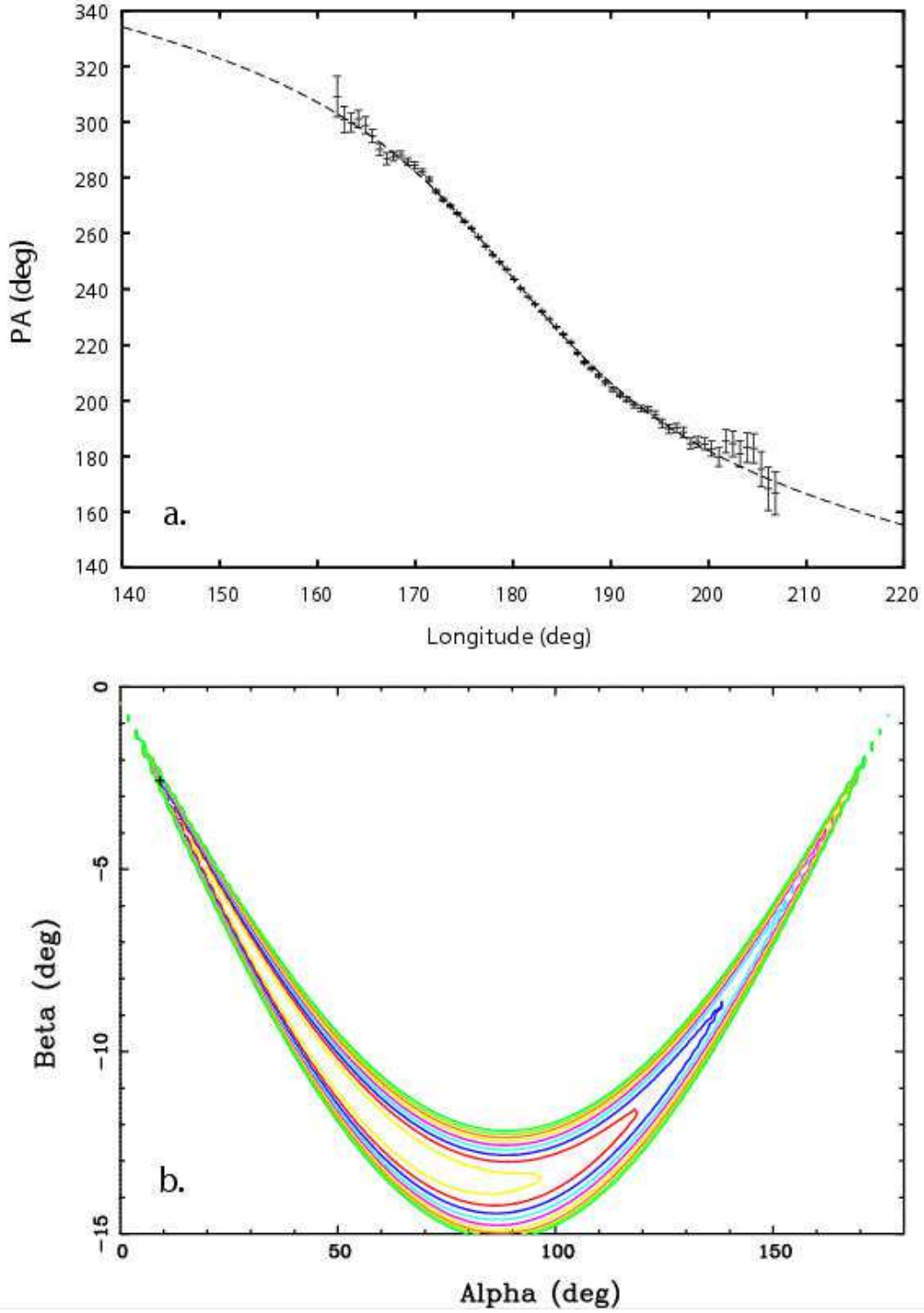


Fig. 2.— Fit of polarization data of PSR B0628-28. The upper panel **a.** shows the polarization position angle at 1400 MHz. The lower panel **b.** shows  $\chi^2$ -contours of the rotating vector model fit. The global maximum is indicated by a + sign. Alpha and Beta are the inclination and impact angles.



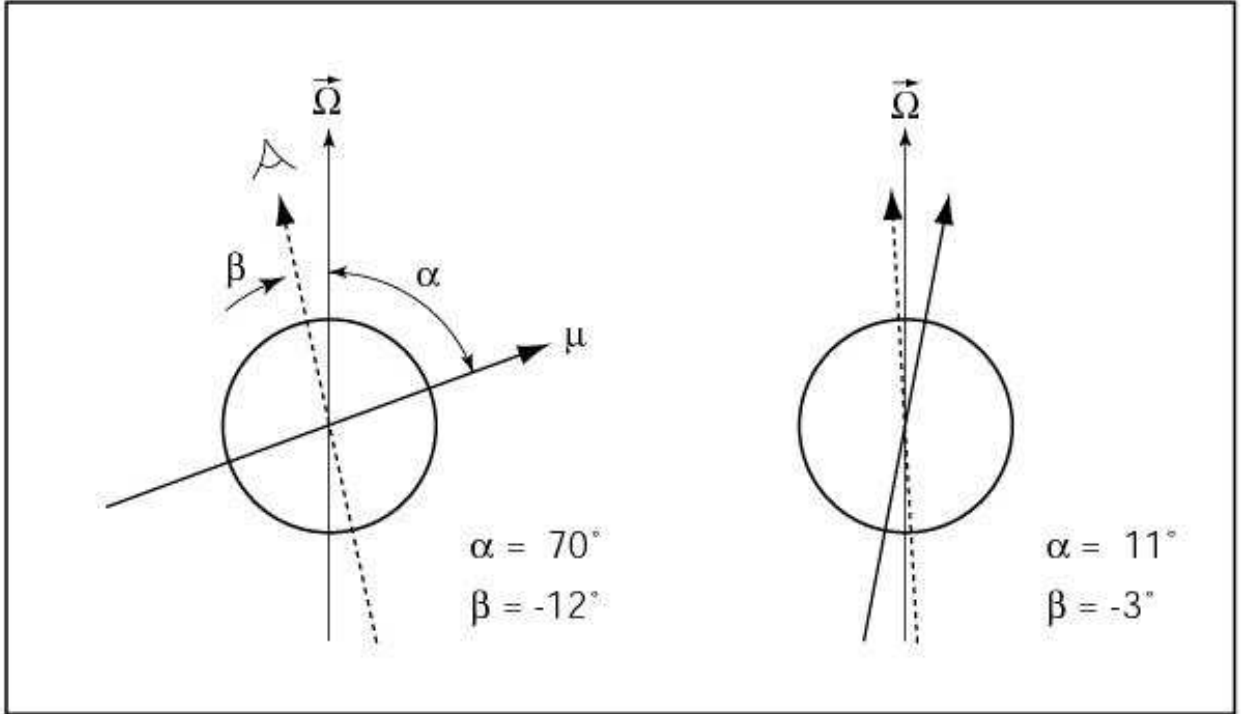


Fig. 3.— Possible emission beam geometries of PSR B0628–28 as deduced from fitting the rotating vector model to the polarization angle swing observed at radio frequencies.  $\alpha$  is the inclination of the magnetic axis,  $\beta$  the minimum angle between the magnetic axis and the line of sight.  $\vec{\Omega}$  is the rotation axis.

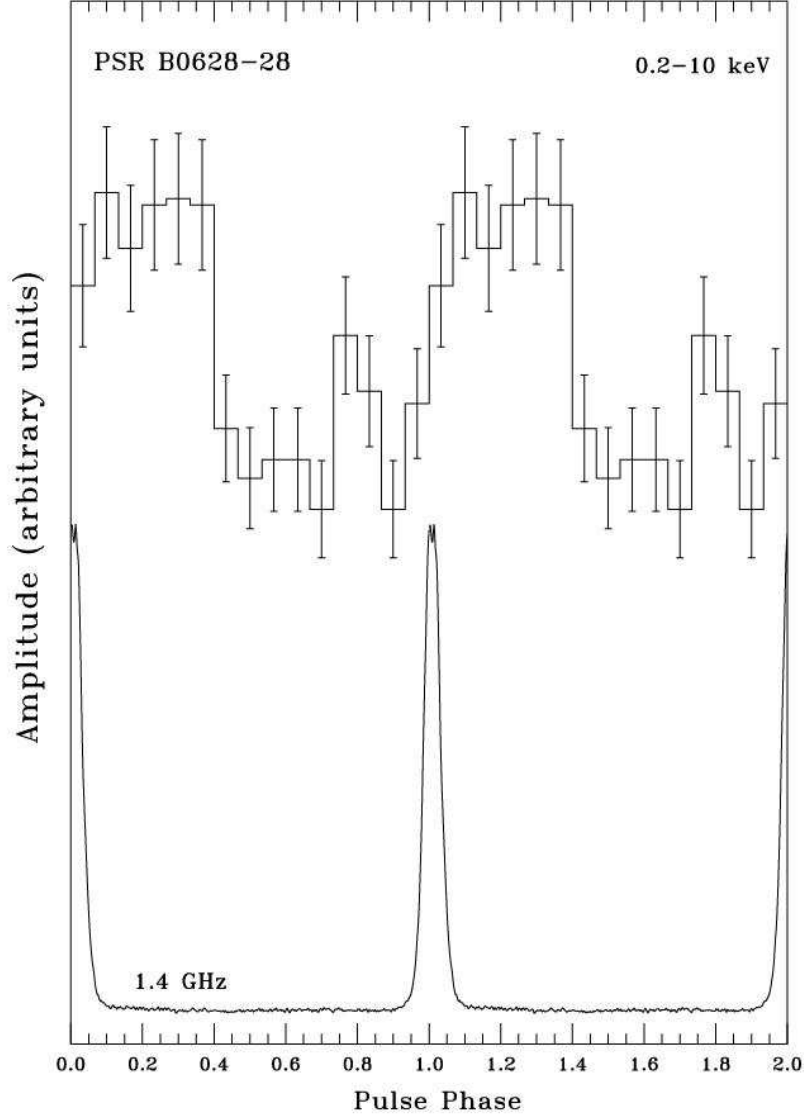


Fig. 4.— Integrated pulse profiles of PSR B0628-28 as observed in the 0.2 – 10 keV band (top) and and at 1.4 GHz with the Jodrell Bank radio observatory (bottom). X-ray and radio profiles are phase related. Phase zero corresponds to the mean epoch of the XMM-Newton observation. Two phase cycles are shown for clarity.

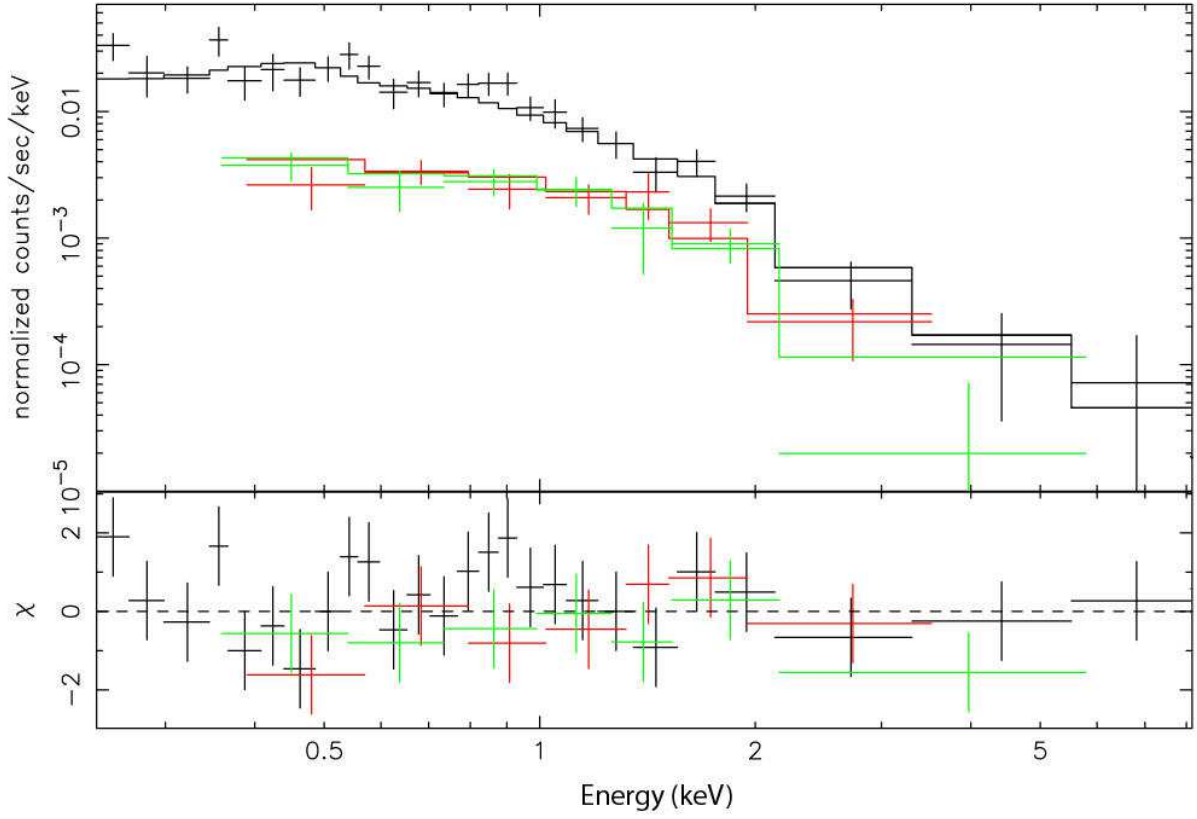


Fig. 5.— Energy spectrum of PSR B0628–28 as observed with the EPIC-PN (upper spectrum) and MOS1/2 detectors (lower spectra) and simultaneously fitted to an absorbed power law model (*upper panel*) and contribution to the  $\chi^2$  fit statistic (*lower panel*).

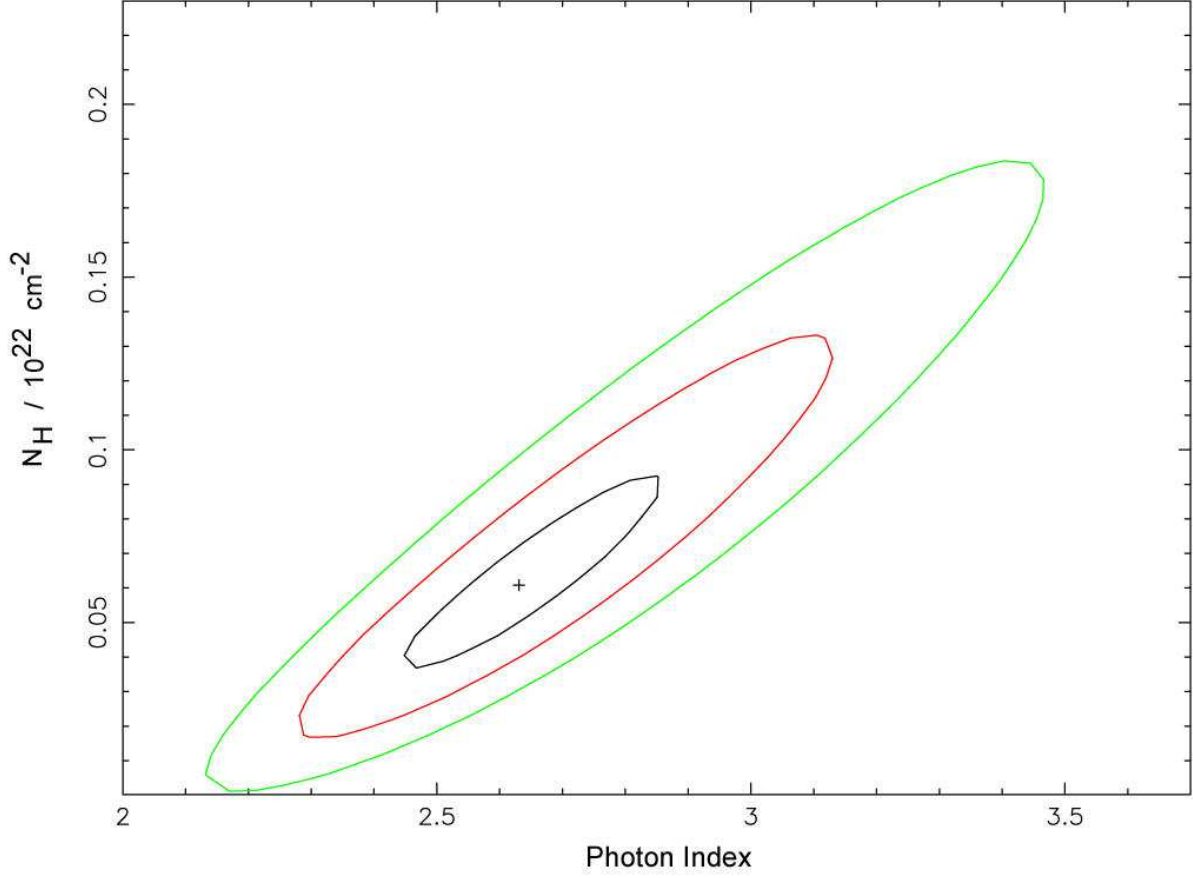


Fig. 6.— Contour plot showing the relative parameter dependence of the photon index vs. column absorption for the power law fit to the PSR B0628–28 data. The three contours represent the  $1 - \sigma$ ,  $2 - \sigma$  and  $3 - \sigma$  confidence contours for one parameters of interest. The ‘+’ sign marks the best fit position, corresponding to  $\chi^2_{min} = 0.8650$  for 40 dof.

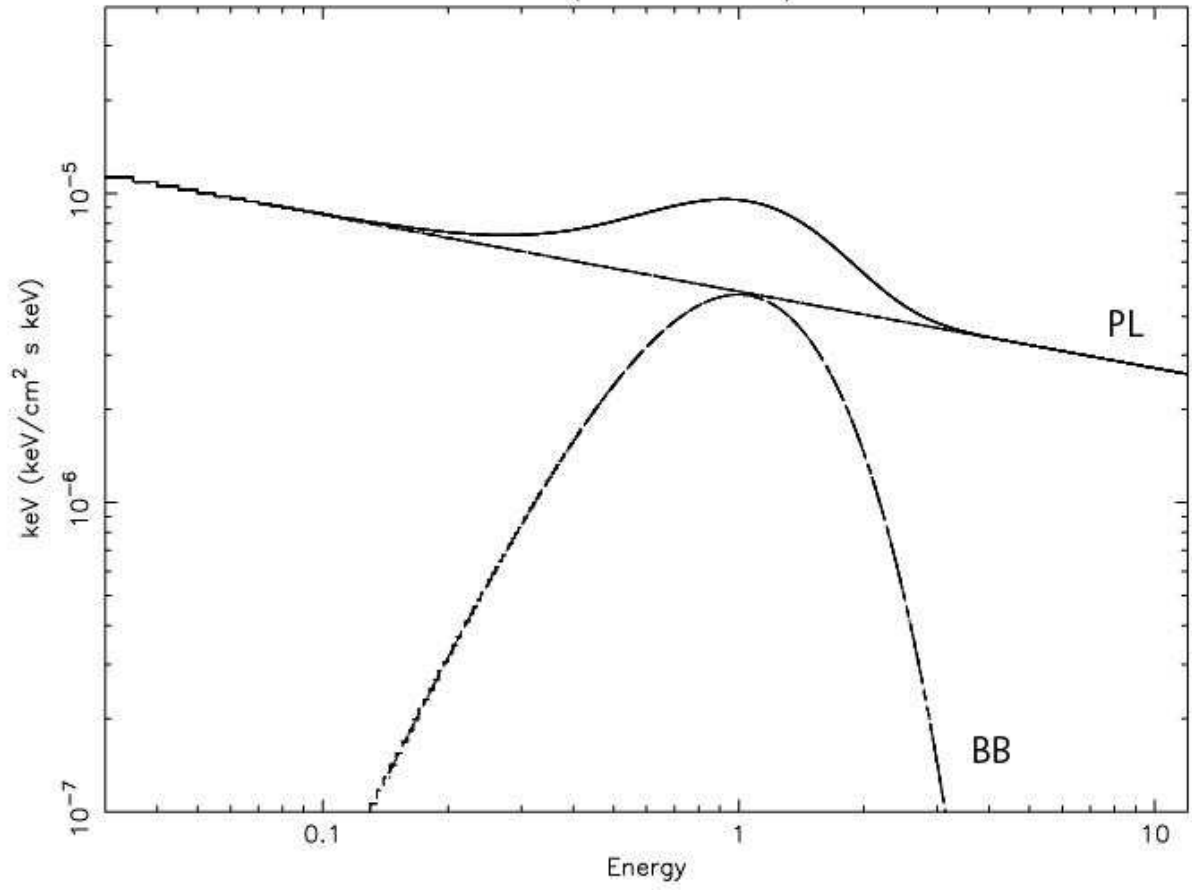


Fig. 7.— Blackbody plus power law spectral components and combined model as fitted to the spectral data of PSR B0628–28.

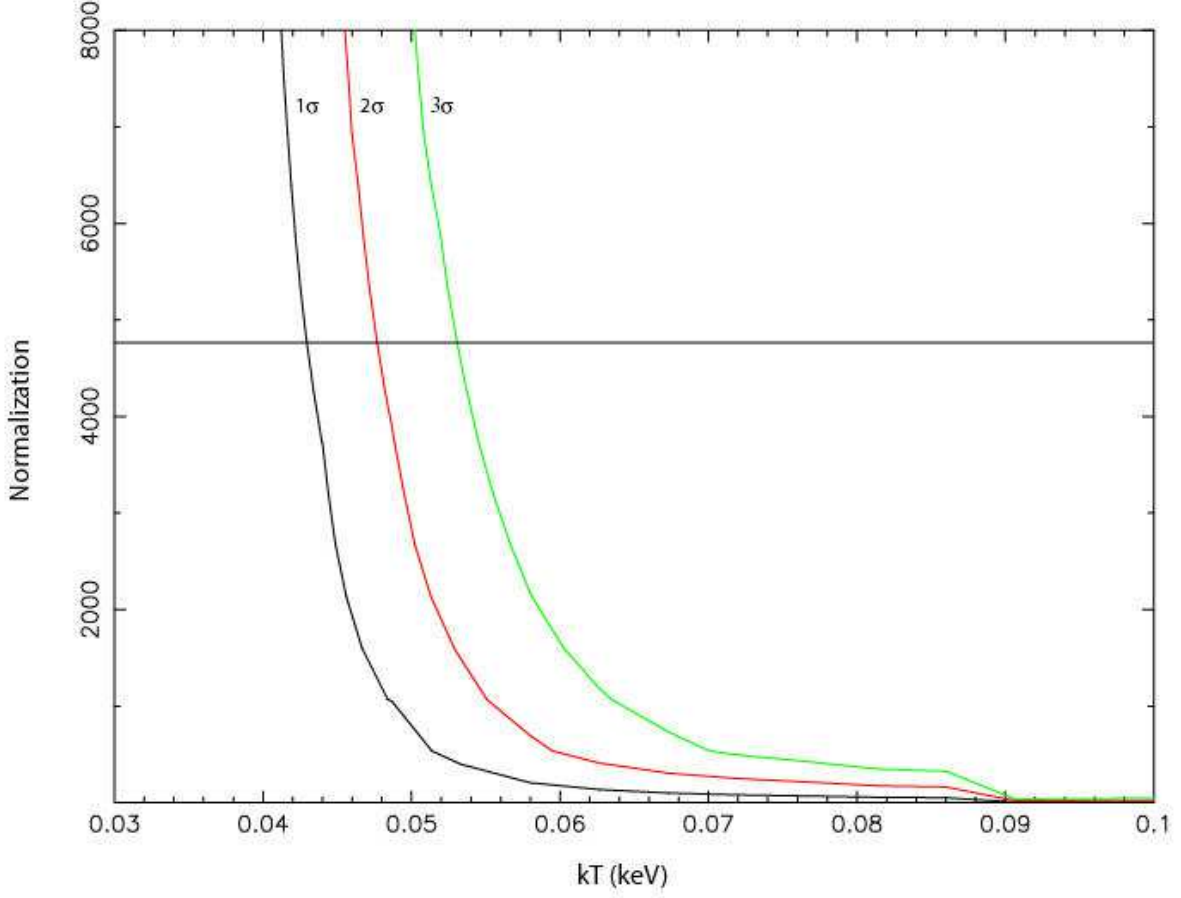


Fig. 8.— Portion of the confidence contours showing the blackbody normalization versus blackbody temperature for the composite Planckian plus power law model (see text). The horizontal line at a normalization of 4772 corresponds to a neutron star radius of 10 km at a pulsar distance of 1.45 kpc. The contours correspond to  $\chi^2_{min} = 33.91$  plus 2.3, 6.17 and 11.8 which are the  $1 - \sigma$ ,  $2 - \sigma$  and  $3 - \sigma$  confidence contours for 2 parameters of interest.

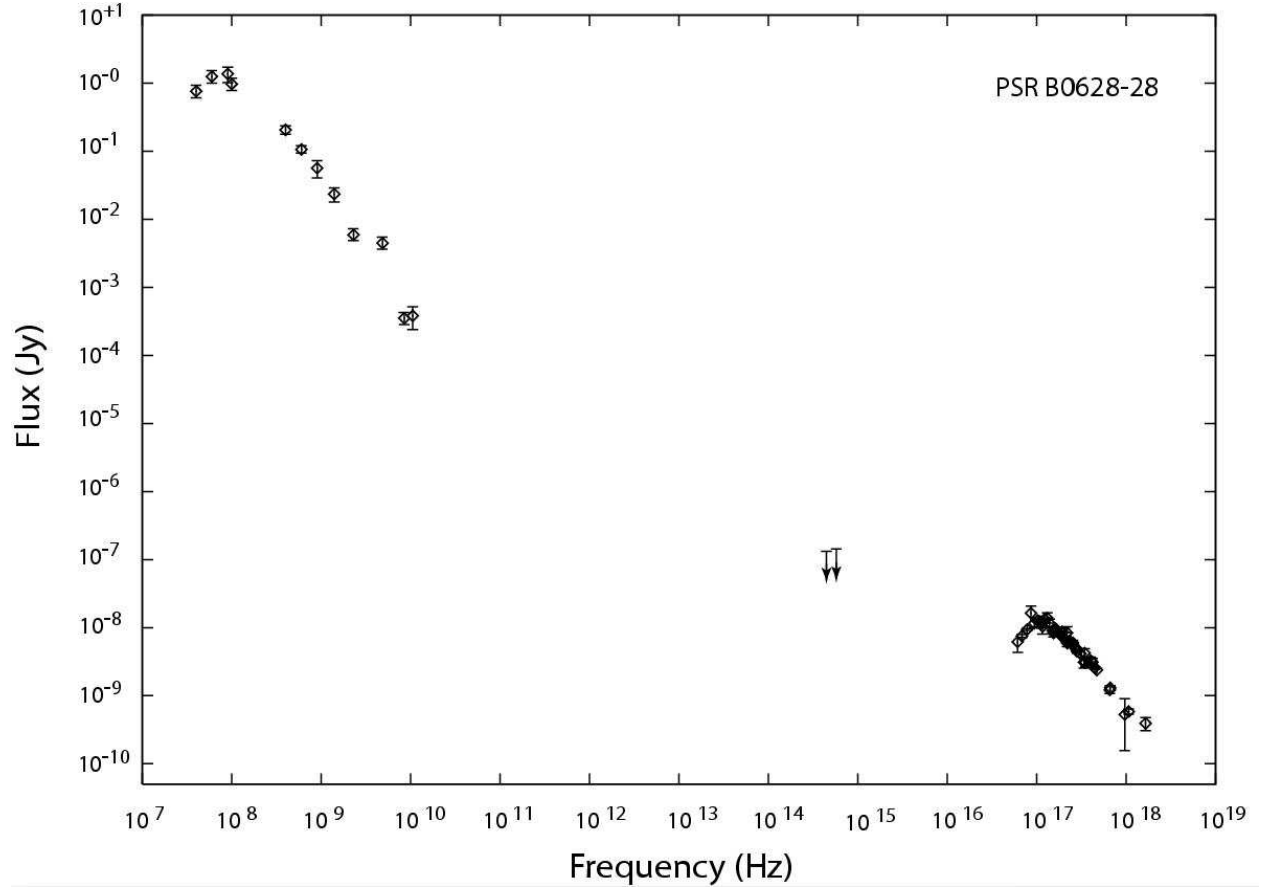


Fig. 9.— Combined radio, optical and X-ray spectral data of PSR B0628–28.